Lord, N., Wang, H., and Fratta, D. (2016). "A Source-Synchronous Filter for Uncorrelated Receiver Traces from a Swept-Frequency Seismic Source". Geophysics. DOI: 10.1190/geo2015-0324.1.

# A Source Synchronous Filter (SSF) for Uncorrelated Receiver Traces from a Swept-Frequency Seismic Source

Neal Lord, Herb Wang, Dante Fratta[1]

Geoscience and Geological Engineering; University of Wisconsin-Madison. Madison, WI 53706. USA

**Abstract:** This paper presents a novel algorithm to reduce noise in signals obtained from swept-frequency sources by removing out-of-band external noise sources and distortion caused from unwanted harmonics. The algorithm is designed to condition non-stationary signals for which traditional frequency-domain methods for removing noise are less effective. The Source Synchronous Filter (SSF) is a time-varying narrow-band filter, which is synchronized with the frequency of the source signal at all times. Because the bandwidth of the filter needs to account for the source to receiver propagation delay and the sweep rate, SSF works best with slow sweep rates and move out adjusted waveforms to compensate for source-receiver delays. The SSF algorithm was applied to data collected during a field test at the University of California Santa Barbara's Garner Valley Downhole Array site in southern California. At the site a 45-kN shaker was mounted on top of a 1-story structure and swept from 0 to 10 Hz and back over 60 seconds (producing useful seismic waves above 1.6 Hz). The seismic data were captured with small accelerometer and geophone arrays and with a Distributed Acoustic Sensing (DAS) array,

[1] Corresponding author. Geological Engineering. University of Wisconsin-Madison. Madison, WI 53711. E-mail address: fratta@wisc.edu.

which is a fiber-optic based technique for the monitoring of elastic waves. The result of the application of SSF on the field data is a set of undistorted and uncorrelated traces that can be used in different applications, such as measuring phase velocities of surface waves or applying convolution operations with the encoder source function to obtain travel times. The results from the SSF were used with a visual Phase Alignment Tool (PAT) to facilitate developing dispersion curves, and as a pre-filter to improve the interpretation of the data.

**Keywords:** filtering, signal processing, surface waves, Vibroseis.

## Introduction

Vibroseis and other swept-frequency seismic sources are used widely in subsurface exploration. A standard practice is to cross correlate the source signal with the received signals. One problem is that a significant source of noise is caused by the distortion from upper harmonics generated by seismic vibrators. These harmonic distortions decrease signal-to-noise ratio and have been addressed both during data acquisition as well as in processing (Abd El-Aal, 2010). In addition, noise from sources such as traffic vibration can be a problem particularly in the low frequency range. For those types of noise traditional frequency domain filters are difficult to apply, in particular for dispersed waves where the frequency content and statics change with time at the receiver. More sophisticated methods of spectral decomposition have been tried, such as filtering in F-T space (Okaya et al., 1992) or Short Time Fourier Transform (STFT), or sliding-window analyses (Chakraborty and Okaya, 1995); however these techniques can be ad hoc and are not always successful. This paper takes advantage of the data in the uncorrelated domain to filter and remove noise from harmonics and traffic.

The purpose of this paper is to describe a novel SSF which rejects unselected harmonics and other out-of-band noise in the received signal. The SSF assumes that the frequency of the receiver trace at any time is within a narrow frequency band centered on the frequency of the swept-frequency source. The SSF is a time-varying filter that produces a receiver trace that is free of source harmonics and other noise sources outside of the narrow band filter centered on the source frequency. The resulting, undistorted, uncorrelated trace can then be used in different applications, such as for surface-wave dispersion analysis by following a particular phase across a receiver array or for travel-time analysis by convolving the receiver trace with the encoder source function.

The details of the SSF and its applications are described in the context of a field test carried out over several days in September 2013 at the University of California-Santa Barbara's Garner Valley Downhole Array (GVDA) site (nees@UCSB, 2014) in the San Jacinto Mountains in southern California. At the site, we collected Distributed Acoustic Sensing (DAS) data, a fiber-optic technique that senses seismic waves on the direction of the fiber at one-meter intervals. These data provide a much higher density of sensors than can typically be obtained in near-surface geophysical studies and therefore it requires a novel tool for the rapid and efficient signal processing of the data.

The SSF method was applied to traces collected from a variety of sensors in which the University of California-Los Angeles's AFB Model 4600A semi-custom 45-kN eccentric mass shaker (nees@UCLA, 2014) mounted on the concrete slab of the top floor of the Garner Valley's one-story "Mini-Me" structure was used as a seismic source. The sensors included 762 m of Distributed Acoustic Sensing (DAS) cable, a 48-channel seismometer array, several

accelerometers, and GVDA borehole seismometers. The shear shaker was programmed to provide a linear frequency sweep from 0 to 10 Hz and back to 0 over a 60-second period. Energy is 0 at 0 Hz, increases with frequency to the structure resonant frequency (5.5 Hz), and then is flat to the maximum frequency (10 Hz). Useful seismic energy is produced at 1.6 Hz and above. As with Vibroseis trucks, the shaker mounted on the "Mini-Me" structure generated several harmonics, which contaminated the received traces (Bagaini, 2010).

This paper first introduces the time-varying SSF methodology, describes the field setup, the DAS array and data acquisition methodology, and then presents the implementation of the time-varying SSF methodology to the data collected by the DAS array at Garner Valley site. Although the ground motion data were much stronger for arrivals associated with the primary source frequency, SSF filtering permitted the analysis of not only the fundamental frequencies but also of several harmonics to extend the frequency range of the phase velocity dispersion curve of the Rayleigh wave. The higher-quality filtered traces also allowed the development of a Phase Alignment Tool (PAT), which provides the user with a visual means to align a particular phase. The filtered traces also improved results when applying techniques such as Moving Window Cross Correlation (MWCC - Sun et al., 2009) and Multichannel Analysis of Surface Waves (MASW -Park et al., 1999).

**Single-Sideband SSF Algorithm**

The SSF algorithm applies to ground-motion sensors that are responding to a sinusoidal source whose time-varying frequency is known. The algorithm is designed to reject noise in the received signal at a time $t$. The rejected noise is outside of a narrow frequency band centered on

the source frequency at the same time *t*. This frequency band is user defined but should accommodate the change in source frequency that occurs as a result of the propagation time between source and receiver, that is, the change in frequency source is the product of the lag time and the sweep rate of the source. Consequently, the method works best for slow sweep rates and for move out adjusted waveforms. The SSF has characteristics of a multiple filter technique in which a narrow-band filter is applied to individual receiver traces at a sequence of center frequencies (Gabriels et al., 1987; Dziewonski and Hales, 1972). However, a key concept of the SSF is that the narrow-band filter is centered at a fixed frequency, $f_{NBF}$, rather than using a bank of filters. Having a single center frequency is achieved using Single Sideband modulation to shift the receiver signal to the fixed narrow-band filter frequency, $f_{NBF}$. Using the analogy of single sideband radio, $f_{NBF}$ plays the role of the intermediate frequency and $f_{LO}$ plays the role of the carrier frequency. The SSF algorithm is continuously 'tuning' the $f_{LO}$ to the changing source frequency and shifting the frequency to the upper sideband frequency, $f_{NBF}$. The frequency $f_{NBF}$ can be chosen somewhat arbitrarily but must be outside the range of information. The single sideband modulation requires a local oscillator that is multiplied (also known as heterodyned or mixed) with the receiver signal, i.e., the sensor signal is multiplied by the local oscillator.

$$2 \cdot \sin(2\pi \cdot f_{SRC} \cdot t) \cdot \sin(2\pi \cdot f_{LO} \cdot t) = \cos[2\pi \cdot (f_{SRC} - f_{LO}) \cdot t] - \cos[2\pi \cdot (f_{SRC} + f_{LO}) \cdot t] \quad (1)$$

where $f_{SRC}$ is the frequency of the source at time *t*. The trigonometric identity on the right hand side of Eq. 1 shows that mixing two frequencies produces a beat frequency and a sum frequency, which are known as the lower and upper sidebands, respectively. The lower

sideband can be removed by phase shifting both the receiver signal and the local oscillator by 90° and subtracting their product from Eq. 1. This is the upper sideband modulator. A Hilbert transform is used to shift the receiver signal by 90°. Similarly the upper sideband can be removed by phase shifting both the receiver signal and the local oscillator by 90° and adding their product to Eq. 1. This is the upper sideband demodulator. The upper sideband frequency is targeted to be *fNBF.* The local oscillator is chosen to shift the source frequency to *fNBF* and to be phase-locked with the swept-frequency source. These constraints are implemented in the algorithm by calculating the phase of the local oscillator at time *t* by

$$\theta_{LO} = \theta_{NBF} - \theta_{SRC} \tag{2}$$

where $\theta_{NBF} = 2\pi \cdot f_{NFB} \cdot t$ and $\theta_{SRC} = \int_0^t 2\pi \cdot f(t) \cdot dt$, that is, $\theta_{SRC}$ is computed by integrating $2\pi$ times the sweep frequency from zero to time *t*. The result of the upper sideband modulator is to shift the signal frequency at time *t* to the upper sideband frequency, *fNBF,* where a high-order, zero-phase, narrow band filter is applied and an upper sideband demodulator shifts the signal back down to the original source frequency. The SSF is an example of a time-frequency filter because it affects the signal in frequency-time space. The flow diagram is presented in Fig. 1, which shows the core of the SSF routine. Of special note is that the process is performed in the time domain (with the exception of the Hilbert transform which uses the Fourier transform and its inverse to efficiently compute the 90° phase shift).

**GVDA Field Layout**

The University of California – Santa Barbara's site at Garner Valley was developed to improve the understanding of the effects of surface geology on strong ground motion. The site includes surface and borehole accelerometers, and pore pressure transducers to record strong ground motions, excess pore pressure generation, and liquefaction response of subsurface soils. The site also includes two one-story tall structures used to evaluate soil-foundation-structure interaction effects for Geotechnical and Structural Earthquake Engineering studies. The site is located in a seismically active region between the San Jacinto Fault 7 km to the west and the San Andreas Fault 35 km to the east in a narrow valley within the Peninsular Ranges Batholith in California. The near-surface soil-to-bedrock structure is well characterized (nees@UCSB, 2014). Alluvial, silty and sandy soils extend to about 16-m depth. They overlie weathered bedrock down to unweathered granodiorite at a depth of 88 m.

The main sensor array used in this study is formed by a fiber optic cable that is interrogated with a laser pulse. The backscattered light from the laser signal is interpreted to sense the dynamic strain rate along the axis of the cable (Parker et al., 2013; Castongia et al., 2015). The DAS array senses the strain rate caused by a propagating wave by dynamically monitoring the relative displacement of scattered in the fiber optic cables along a section of the cable (i.e., gauge length – Daley et al. 2015). DAS displays the strain rate responses in sensor channel separated by 1 m and sampled at 1 kHz. DAS sensors have strong directivity, it senses strain rates only in the direction of the fiber cable (Mateeva et al., 2014).

A linear length of 762 m of fiber cable, deployed in a trench varying in depth from about 0.15 to 0.46 m, formed the DAS array layout (Fig. 2). The trench was backfilled and compacted

148 to provide coupling between the fiber-optic cable and surface soil. The sensor distance was
149 doubled to 1524 m because two internal strands within a single jacket were spliced together at
150 the end of the cable. To complement the DAS array, seven tri-axial accelerometers and a 48-
151 channel seismometer array from the Portable Array Seismic Studies of the Continental
152 Lithosphere (PASSCAL) instrument pool were deployed on the source and along segments of
153 the two subdiagonals. The equipment included 7 Kinemetrics EpiSensor tri-axial
154 accelerometers, two Kinemetrics Granite digitizers, two Geometrics GEODE 24-channel
155 seismographs and 18 triaxial 4.5 Hz L-28-3D geophones.

156 We use the data collected at Garner Valley to test the SSF. The DAS data presented for the
157 SSF analysis utilized the University of California – Los Angeles' eccentric mass shaker placed on
158 the top floor of the "Mini-Me" structure (Fig. 3a). We selected this source because it was well
159 characterized, it provided a strong shear wave, and it was available for academic research at a
160 site well-suited to a field trial of DAS. The mass shaker could generate significant amplitude
161 surface waves in the direction of the main orientation of the DAS array in the low frequency
162 range. Accelerometers on the top of the "Mini-Me" slab recorded the source signal. The
163 vibration of the shaker on the "Mini-Me" structure generated a vertically-polarized shear wave
164 that concentrated radiated energy in an approximately west-to-east direction. External
165 triggering and GPS timing between the shaker, DAS, and the PASSCAL Geode seismograph
166 were used to synchronize clocks between the different systems. The shaker was swept from its
167 at-rest position to 10 Hz and back to the at-rest position over 60 seconds (Fig. 3b). Fig. 4 presents
168 the time and frequency domains responses of the shaker, the DAS response, and the horizontal
169 components of the PASSCAL geophone rotated into the direction parallel to the adjacent DAS

fiber-optic cable. It should be noted that geophones and DAS channels sense different physical quantities. Geophones measure particle velocities, while DAS channels sense strain rates along gauge length (i.e., 10 m in the case of this dataset - Daley et al., 2015). Furthermore, DAS has very strong strain rate directivity (maximum in the direction of the fiber and zero in the direction perpendicular to the fiber -Mateeva et al., 2014). The geophone and DAS waveforms are from receivers 175 m from the mini-me source and contain both surface wave and reflected and refracted P-waves arrivals which travel at different velocities and interfere with each other. Both different sensing mechanisms and the presence of different modes of propagation explain in part the difference in the geophone and DAS responses presented in Fig. 4b and 4c. Additionally conversion of DAS strain rate to particle velocity by integrating records in time and space yield similar responses to geophones as reported by Daley et al. (2016).

**Application of Single-Sideband SSF Algorithm in Seismic Data**

The step-by-step application of the Single Sideband - SSF algorithm is illustrated in Fig. 5 for the shaker on the "Mini-Me" structure source and DAS sensor channel whose time series is shown in Fig. 4c. In the case of the shaker on the "Mini-Me" structure, the mass shaker sweeps up from the at-rest position to 10 Hz over 30 seconds and back to the at-rest position over the next 30 seconds. If the maximum travel time is one second, then the maximum frequency by which the received signal lags the source signal is 0.33 Hz on the upsweep and leads the source signal by the same 0.33 Hz on the downsweep. Therefore, the minimum Narrow Band Filter bandwidth is 0.66 Hz.

The left figure in each pane is the spectrogram for the frequency range from 0 to 500 Hz whereas the right figure in each pane presents the magnification of a 50 Hz band within the full spectrogram.

a. The spectrogram of the unfiltered DAS time series shows the sweep signal, which goes from the at-rest position to 10 Hz and back to the at-rest position, and its harmonics. Vehicle noise appears near 10 seconds and again near 57 seconds with energy between about 6 and 50 Hz. Upwards of a dozen harmonics of the fundamental frequency appear in the full spectrogram in the left pane of each figure set with an expanded view of the first five harmonics shown in the right pane.

b. A broad zero-phase band-pass filter is applied to the received waveform which passes the entire frequency range of interest while removing signals near the fixed narrow band filter frequency. This initial band pass was chosen to be between 0.4 and 30 Hz. The zero-phase filter is implemented by applying a Butterworth filter twice: first in the forward time direction and then in the time reverse direction. The first and second harmonics are still strongly present.

c. The source signal and the local oscillator are used with an upper sideband modulator to shift the signal to the upper sideband frequency, which was chosen to be the center of the narrow band filter, $f_{NBF}$ = 350 Hz. Because the local oscillator frequency is adjusted to the fundamental source frequency to sum to 350 Hz, the signal is centered on the fundamental frequency of 350 Hz. The first and second harmonics are still strongly present.

d. A high-order, zero-phase, narrow-band filter, whose bandwidth is 1 Hz, is applied to the upper sideband frequency signal. Note that the harmonics and other noise outside the 1-Hz band of the source frequency are all removed.

e. The same local oscillator used for upper sideband modulation is now used with an upper sideband demodulator to frequency shift the filtered result back to the baseband. The harmonics and other noise are removed and only the response associated with the fundamental source frequency remains.

**Band-Pass Filtering vs. SSF**

The example presented on the DAS data compares the results in the time domain of a Band Pass Filter versus the SSF. Fig. 6a shows 10 seconds of raw data recorded by the entire DAS array for the swept-frequency source described previously. The slowly varying wave arrivals come from the shaker source. The incoherent, parabolically-shaped arrivals correspond to arrivals on the array from a passing vehicle. The trace presented on the right in Fig. 6a is the same 10 seconds showing the waveform from a single sensor channel (i.e., channel 575). This trace clearly shows the high-frequency noise from the passing vehicle. Fig. 6b shows the same plot after the raw data have been filtered with a simple 0.4-to-12-Hz band-pass filter, where the 0.4 Hz cut-off was chosen to remove the very low frequency components and the 12 Hz cut-off was chosen to be far enough away from the 10-Hz maximum frequency of the source. The band-pass filter has clearly removed the very low frequencies in the records (vertical stripes in the left pane of Fig. 6a), and a majority of the energy from the passing vehicle (12 Hz and higher) but the in-band (~6 Hz to 12 Hz) frequencies still remain. Both the fundamental

frequency and its first harmonic are visible in the waveform. As the collected surface waves are dispersive, the frequency-dependent travel times distort the wave shape of the received signal. Fig. 6c again shows the same plot but after the raw data have been filtered using the SSF. This figure also has clearly removed the very low frequency components (vertical stripes in the left pane of Figure 6a), and much more of the energy from the passing vehicle. The SSF passes only the fundamental frequency of the swept-frequency source, except at a sweep frequency of 1 Hz when both the fundamental and the first harmonic are in the pass band of the narrow band filter. The SSF allows higher order harmonics of the swept source to be filtered separately by using integer multiples of the source phase angle as the source signal and adjusting the bandwidth of the narrow band filter. The reduction of noise from a filter bandwidth of 11.6 Hz (0.4-to-12 Hz) using only a Band Pass Filter to a filter bandwidth of 1 Hz in the SSF corresponds to an increase in signal-to-noise ratio of the square root of the ratio 11.6 Hz/1 Hz, or a factor of 3.4. As shown in the wiggle trace in Fig. 6c, the ability of the SSF to separate the swept-source fundamental frequency from higher order harmonics and other noise leads to a clean, uncorrelated time series for the received waveform. The application of the proposed algorithm is extended to geophone responses. Fig. 7 shows how the SSF is able to remove not only the high frequency noise but also the traffic noise that was captured by the PASSCAL vertical geophone closest to the DAS channel 575 shown in Fig. 6. The waveform treated with the SSF (Fig. 7c) shows a much higher signal to noise ratio than bandpass filtered waveform (Fig. 7b) as the traffic noise is almost completely removed.

**Velocity Dispersion Analysis**

A major motivation for developing the SSF algorithm was to determine phase-velocity dispersion curves of surface waves along the DAS and seismometer arrays at Garner Valley Downhole Array site using methods such as MASW or MWCC (Park et al., 1999; Sun et al., 2009; Baldwin et al., 2014). The undistorted waveforms following application of the SSF algorithm make it relatively easy to follow visually a particular phase of a waveform over many sensor channels. Further, the separation of source harmonics in the received waveforms allows for the determination of the velocity dispersion by extending the range of frequencies to higher order harmonics.

Figure 8_are the Mini-Me shaker source accelerometer cross correlated with the DAS receiver channels along the long line and along the nearest sub-diagonal line after whitening both the source and received waveforms. In the long line parallel (and furthest) to the road there are two arrivals: A strong surface wave with an apparent velocity of 180 m/s and a weaker arrival with an apparent velocity of 500 m/s. Both have linear move out which is consistent with a surface wave, a direct arrival, or a refractor with shallow depth. In the near sub-diagonal line the arrivals are more complicated. The fastest arrival has a linear move out velocity of 350 m/s. The strongest arrival has an apparent velocity of 215 m/s but increases to 350 m/s at about 65 m from the start of the line. There does seem to multiple waves interfering with each other. Along the diagonal line, the DAS cable is sensitive to both the radial component of the Rayleigh wave and the transverse Love wave.

Special care needs to be taken with using the velocity dispersion analysis for uncorrelated data in the presence of such interfering surface wave modes. The method will follow the phase

change between channels for the highest amplitude surface-wave at that particular frequency, but it can easily skip between modes. For this reason, it is recommended that the method only be used for low frequencies and for short offsets. At longer offsets and at higher frequencies, higher-order modes can dominate the amplitude spectra, and the phase alignment will record a mixture of the different modes. Good quality control is required. In our case, we compare the results to those obtained with traditional surface-wave analysis previous spectral analysis of surface wave (SASW) results by Stokoe et al. (2004) and Baldwin et al. (2014).

An interactive, Phase Analysis Tool (PAT) was developed to allow the user to find visually the best-fit phase velocity at different source frequencies by choosing the time interval for waveform analysis across a number of sensors. The tool is shown in Fig. 9 for a DAS profile that is 190-meters long and radially oriented with respect to the shaker source. A one-second time interval is centered at 10 seconds. The source frequency versus time can be calculated using either the mass wheel encoder or using the accelerometer signal. Using the mass wheel encoder data, the source frequency at 10 seconds is 3.24 Hz. The user of the PAT obtains the apparent velocity of a particular phase of the surface wave by adjusting the velocity control so that the waveforms appear flat at the grey cursor line (line at 10 seconds). In Fig. 8a, only a 0.4 - 12 Hz bandpass filter has been applied to the waveforms. Noise and harmonics from the swept-frequency source make it difficult to evaluate which velocity best fits the data. In Fig. 8b, the SSF algorithm has been applied. The band-pass filtered traces are significantly improved. Then the best-fit phase velocity of 418 m/s can be chosen. By repeating the process at different arrival times, corresponding to several source frequencies, the surface wave apparent velocity vs. period curve can be obtained. The dispersion-curve results for the DAS profile collected at the

298 Garner Valley Downhole Array site are shown in Fig. 10. Rayleigh wave velocities increase
299 significantly at lower frequencies and, hence, longer wavelengths, because S-wave velocity
300 increases with depth in the unconsolidated alluvial deposits at Garner Valley. This curve is
301 extended to the higher frequency range by using higher harmonics. The dispersion curve
302 obtained with the DAS array and reduced with the proposed SSF algorithm compare well with
303 previous spectral analysis of surface wave (SASW) results by Stokoe et al. (2004) and Baldwin et
304 al. (2014). While the low frequency (< 10 Hz) results are not a perfect match at the low frequency
305 range (datasets were collected along different lines where depths to the weathered bedrock are
306 likely to be different), the high frequencies results show a good match. High-frequency surface
307 waves sense shallower uniform alluvial deposits and the phase velocity is very similar
308 regardless of the location of the arrays.
309
310 **Summary and Conclusions**
311 This paper presents the SSF algorithm. This novel algorithm was developed for the
312 reduction and interpretation of signals obtained from swept-frequency sources, which contain
313 significant noise from upper source harmonics and environmental noise. The algorithm is
314 designed to reject noise in the received signal throughout its trace outside a narrow frequency
315 band centered on the source frequency at each time. The method works best for slow sweep
316 rates and for move out adjusted waveforms. The proposed technique was applied to data
317 collected at the University of California Santa Barbara's Garner Valley Downhole Array site
318 where ground-motion sensors captured signals from a shaker with a known time-varying
319 frequency function. Results show how the SSF algorithm successfully removed traffic noise and

upper harmonics generated by the shaker source. Furthermore, the proposed algorithm can be applied for the interpretation of dispersion of surface wave propagation. The application of the algorithm yields undistorted waveforms that allow visually following particular phases of a waveform over many DAS sensor channels. Furthermore, the separation of source harmonics in the received waveforms helps in the determination of phase velocity dispersion curves by extending the range of frequencies to higher values.

**Acknowledgments**

This project was supported in part by the National Science Foundation grant number CMMI-0900663 (Program Director: R. Fragaszy) and by the U.S. Department of Energy (DOE) Geothermal Technologies Office (GTO) grant number DE-EE0006760 (Program Managers: E. Metcalfe and L. Boyd). Alex Baldwin, Ethan Castongia, Athena Chalari, Ruman Karaulanov, Chelsea Lancelle, Bob Nigbor, and James Steidl participated in the data collection and discussion of the results. Their contribution is greatly appreciated.

**References**

Abd El-Aal, A. E. K. (2010), Eliminating upper harmonic noise in vibroseis data via numerical simulation, Geophys. J. Int. **181**, 1499–1509.

Bagaini, C. (2010), Acquisition and processing of simultaneous vibroseis data, Geophysical Prospecting, **58**, 81–99.

Baldwin, J. A., Fratta, D., Wang, H. F., Lord, N. E., Chalari, A., Karaulanov, R., Nigbor, R. L., Lancelle, C., and Castongia, E. (2014), Using Distributed Acoustic Sensing (DAS) for

342 Multichannel Analysis of Surface Waves (MASW) to Evaluate Ground Stiffness, Abstract
343 NS31C-3938 presented at 2014 Fall Meeting, AGU, San Francisco, Calif., 15-19 Dec.
344 Castongia, E., Wang, H. F., Lord, N., Fratta, D., Mondanos, M., and Chalari, A. (2015). An
345 Experimental Investigation of Distributed Acoustic Sensing (DAS) on Lake Ice. Journal of
346 Environmental and Engineering Geophysics (under review)
347 Chakraborty, A. and Okaya, D. (1995). Frequency-time decomposition of seismic data using
348 wavelet-based methods, Geophysics, **60**, no. 6, 1906-1916.
349 Daley, T. M., Miller, D. E., Dodds, K., Cook, P. and Freifeld, B. M. (2015). Field testing of
350 modular borehole monitoring with simultaneous distributed acoustic sensing and geophone
351 vertical seismic profiles at Citronelle, Alabama. Geophysical Prospecting, doi: 10.1111/1365-
352 2478.12324
353 Dziewonski, A. M. and Hales, A. L. (1972). Numerical analysis of dispersive seismic waves, ***in***
354 Methods in Computational Physics, B.A. Bolt (ed.), **11**, 217-295, Academic Press.
355 Gabriels, P., Snieder, R., and Nolet, G. (1987). In Situ Measurement of Shear-Wave Velocity in
356 Sediments with Higher-Mode Rayleigh Waves, Geophysical Prospecting, **35**,187-196.
357 Givens, M. J. (2013). Dynamic Soil-Structure Interaction of Instrumented Buildings and Test
358 Structures. PhD Thesis. University of California Los Angeles. 329 pages. Accessed on
359 August 26, 2015: http://escholarship.org/uc/item/3rh1w1hr.
360 Mateeva, A., Lopez, J., Potters, H., Mestayer, J., Cox, B., Kiyashchenko, D., Wills, P., Grandi, S.,
361 Hornman, K., Kuvshinov, B., Berlang, W., Yang Z., and Detomo, R. (2014). Distributed
362 acoustic sensing for reservoir monitoring with vertical seismic profiling, Geophysical
363 Prospecting, **62**, 679–692.

nees@UCSB (2014). Garner Valley Downhole Array. Accessed on May 15, 2015: http://nees.ucsb.edu/facilities/GVDA.

nees@UCLA (2014). Equipment. Accessed on May 15, 2015: http://nees.ucla.edu/equipment.html.

Okaya, D., Karageorgi, E., McEvilly, T., and Malin, P. (1992). Removing vibrator-induced correlation artifacts by filtering in frequency-uncorrelated time space, Geophysics, **57**, 916-926.

Park, C. B., Miller, R. B., and Xia, J. (1999), Multichannel analysis of surface waves, Geophysics, **64**, no. 3, 800–808.

Parker, T., Shatalin, S.V., and Farhadiroushan, M. (2014), Distributed Acoustic Sensing – a new tool for seismic applications, First Break, **32**, no. 2, 61-69.

Stokoe, K. H., Kurtulus, A., and Menq, F.-Y. (2004), Data Report: SASW Measurements at the NEES Garner Valley Test Site, California, 13 January 2004, 12 pp. Accessed on May 15, 2015: http://nees.ucsb.edu/sites/eot-dev.nees.ucsb.edu/files/facilities/docs/GarnerValley-SASWreport.pdf

Sun, L. F., Milkereit, B., and Schmitt, D. R. (2009), Measuring velocity dispersion and attenuation in the exploration seismic frequency band, Geophysics, **74**, no. 2, 113-122.

Wang, H. F., Lord, N. E., A. Chalari, C. Lancelle, J. A. Baldwin, E. Castongia, D. Fratta, R. L. Nigbor, and R. Karaulanov (2014), Field Trial of Distributed Acoustic Sensing Using Active Sources at Garner Valley, California, Abstract NS41C-07 presented at 2014 Fall Meeting, AGU, San Francisco, Calif., 15-19 Dec.

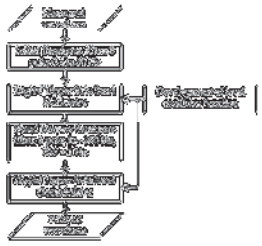

Fig. 1. Block flow diagram for the SSF algorithm.
338x190mm (300 x 300 DPI)

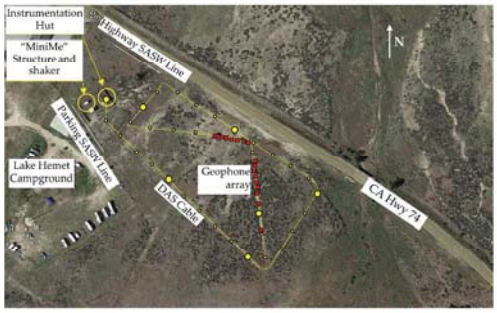


Fig. 2. Location of the Garner Valley Downhole Array testing site and surveyed layout of about 762-m of cable that forms the DAS array. Satellite image from Google Earth. The dots on the DAS cable indicate separations of 20 m. The lines labeled 'Highway' and Parking' correspond to SASW surveys ran by Stokoe et al. (2004).
338x190mm (300 x 300 DPI)

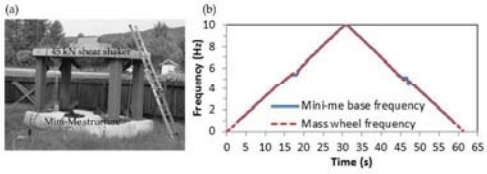


Fig. 3. (a) A University of California Los Angeles 45 kN (10,000 lb. force) shear shaker mounted on the "Mini-Me" structure and its excitation spectrum. The "Mini-Me" structure is a one-story concrete structure composed of a rectangular slab supported by four steel columns. The overall structure is supported by a shallow foundation system The height of the structure is 2.38 m with a concrete base 4.26 m long by 3.13 m wide and 0.61 m thick (Givens 2013) . (b) The source created a vertically polarized shear wave by rocking the "Mini-Me" structure back and forth along the main horizontal axis. The generated shear waves are strongly directed in the EW direction. The 'kinks' in the spectrum at around 5 Hz are caused by structure resonance affecting the loading on the drive motor.
338x190mm (300 x 300 DPI)

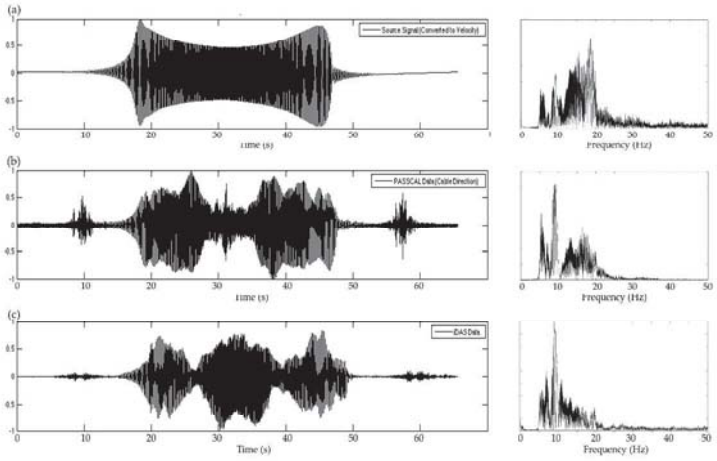


Fig. 4. Time and frequency domain responses of the (a) 45 kN shaker, (b) horizontal geophone, and (c) DAS cable. The geophone and fiber-optic cable were about 1 m apart and about 175 m from the shaker (Wang et al., 2014).
338x190mm (300 x 300 DPI)

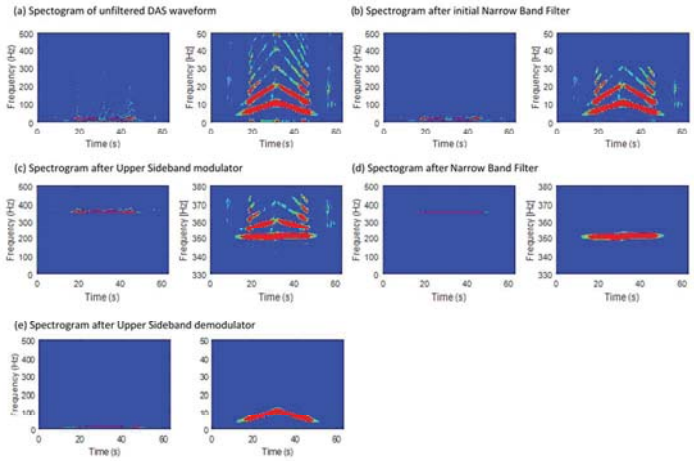


Fig. 5. Frequency-Time spectrograms of the DAS waveforms for the shaker on the Mini-Me structure being swept from rest to 10 Hz and back to test over 60 seconds. The left figure in each pane shows the full frequency range from 0 to 500 Hz while the right figure shows a magnified 50 Hz window of the full spectrum. Each step shows the implementation of the SSF algorithm: (a) the spectrogram of the raw, unfiltered waveform; (b) the spectrogram after a 0.4-to-30 Hz bandpass filter. (c) the spectrogram after Upper Sideband Modulation, (d) Application of the 1-Hz Narrow Band Filter centered at 350 Hz, and (e) the final spectrogram of the filtered DAS response after SSB demodulation.
338x190mm (300 x 300 DPI)

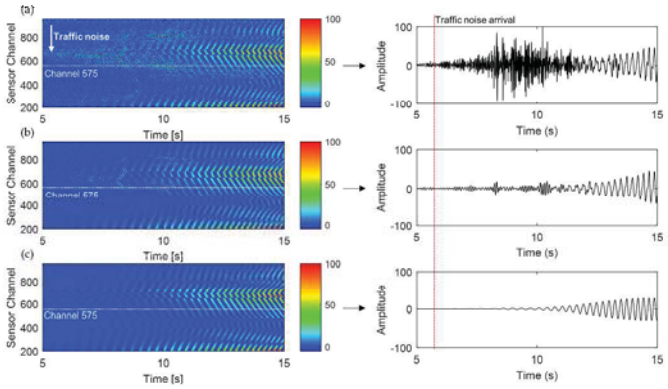


Fig. 6. The left color-intensity plots show the DAS waveforms between 5 and 15 seconds after the start of the sweep over the entire array. The right plots show the time series of the single DAS sensor channel 575. (a) Raw, unfiltered waveforms, (b) Band-pass (0.4 – 12 Hz) filtered waveforms, (c) SSF waveforms. The separation between sensor channels is 1 m.
338x190mm (300 x 300 DPI)

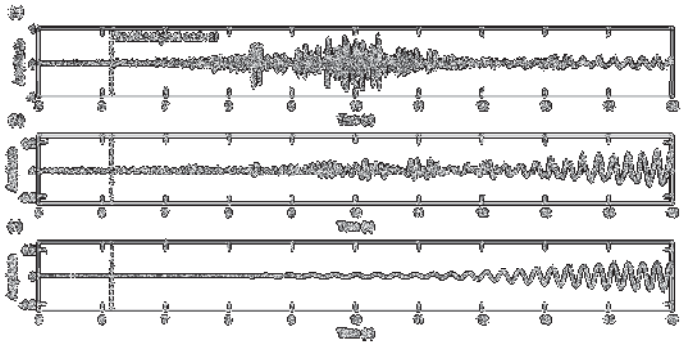

Fig. 7. Example of the application of the proposed SSF algorithm on the vertical PASSCAL geophone closest to the single DAS sensor channel 575. Figures show the geophone waveforms between 5 and 15 seconds after the start of the sweep. (a) Raw, unfiltered waveforms, (b) Band-pass (0.4 – 12 Hz) filtered waveforms, (c) SSFed waveforms.
338x190mm (300 x 300 DPI)

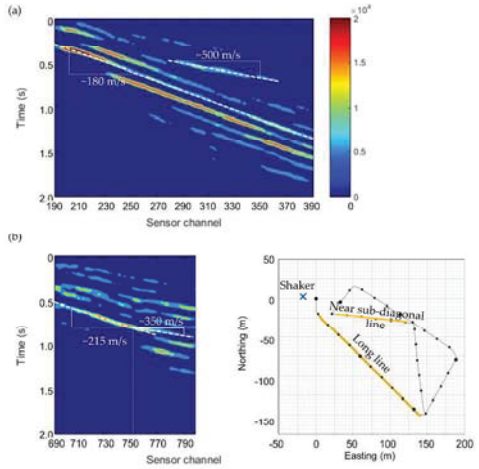


Fig. 8. Mini-Me shaker source accelerometer cross correlated with the DAS receiver channels along both (a) the long line and along (b) the near sub-diagonal line. Whitening was applied to both the source and received waveforms. The separation between sensor channels is 1 m.
338x190mm (300 x 300 DPI)

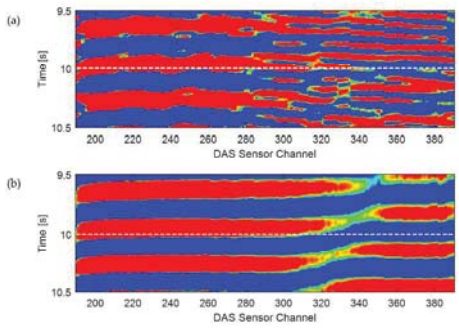


Fig. 9. The PAT allows visual alignment of individual wave phases across a spatial array of receivers. Input parameters include the arrival-time interval and stations selected, the initial Band-Pass Filter and the parameters of the SSF. The phase velocity is determined by adjusting the linear move out velocity until the arrival at the cursor line is horizontal. (a) Simple band-pass (0.4 – 12 Hz) filtered waveforms, (b) SSF filtered waveforms. The separation between sensors is 1 m.
338x190mm (300 x 300 DPI)

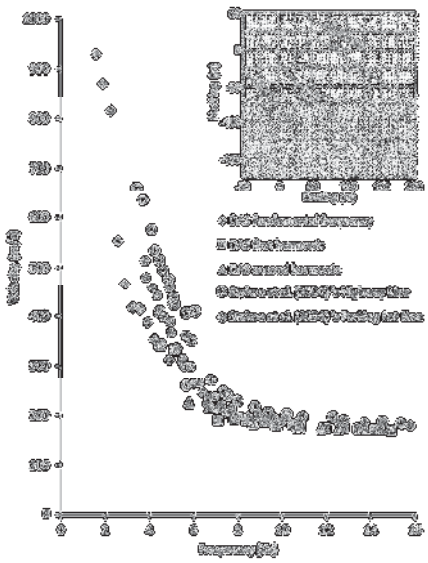

Fig. 10. Surface-wave dispersion curve obtained using the 45 kN swept-frequency shear shaker and the indicated section of the DAS array. Velocities at frequencies above the maximum 10 Hz of the source sweep were obtained using the first and second harmonic generated by the source.
338x190mm (300 x 300 DPI)